Eur. J. Mineral.
2018, **30**, 989–997
Published online 9 May 2018

Honzaite, $(Ni,Co)_2(AsO_3OH)_2(H_2O)_5$, a new Ni-dominant analogue of burgessite, from Jáchymov, Czech Republic

JIŘÍ SEJKORA[1,*], JAKUB PLÁŠIL[2] and ANTHONY R. KAMPF[3]

[1] Department of Mineralogy and Petrology, National Museum, Cirkusová 1740, 19300 Praha 9, Czech Republic
*Corresponding author, e-mail: jiri_sejkora@nm.cu
[2] Institute of Physics ASCR, v.v.i., Na Slovance 1999/2, 18221 Praha 8, Czech Republic
[3] Mineral Sciences Department, National History Museum of Los Angeles County, 900 Exposition Boulevard, Los Angeles, CA 90007, USA

Abstract: Honzaite, $(Ni,Co)_2(AsO_3OH)_2(H_2O)_5$, is a new supergene mineral from the Jáchymov (formerly St. Joachimsthal) ore district, Czech Republic, associated with arsenolite, zeunerite, Ni-rich burgessite and a red amorphous Co–Ni–Cu arsenate phase. It forms pale pink (some with purplish or violet tints) irregular to hemispherical microcrystalline aggregates up to 5 mm in diameter on strongly weathered ore gangue. Tiny prismatic crystals, up to 30 μm long, are rarely observed on the surface of these aggregates. Honzaite has a pale pink streak, a vitreous luster, does not fluoresce under either short- or long-wave ultraviolet light. Cleavage on {0 1 0} is good, the Mohs hardness is ~3, and honzaite is brittle with an irregular fracture. The calculated density is 2.993 g/cm^3. Honzaite is optically biaxial positive, the indices of refraction are α 1.601(2), β 1.608(2), γ 1.629(2), and $2V_{meas.}$ is 60(1)°. Honzaite is monoclinic, space group $P2_1/n$, $a = 4.6736(6)$, $b = 9.296(1)$, $c = 12.592(1)$ Å, $\beta = 99.115(8)°$, $V = 540.2(1)$ Å^3, $Z = 2$. The seven strongest lines in the X-ray powder diffraction pattern are as follows: d (Å)/I(hkl): 7.431/100(0 1 1); 6.215/18(002); 3.717/9(0 2 2); 3.254/7(12$\bar{1}$); 3.078/7(121); 3.005/5(0 3 1) and 2.568/7(1 3 0). The chemical analyses by electron microprobe yielded (in wt%) MgO 0.24, CaO 0.10, FeO 0.21, NiO 16.51, CoO 12.71, CuO 0.55, ZnO 0.84, P_2O_5 0.26, As_2O_5 45.82, SO_3 0.52, $H_2O_{calc.}$ 22.15, total 99.91. The resulting empirical formula on the basis of 13 O atoms per formula unit is $(Ni_{1.08}Co_{0.83}Zn_{0.05}Cu_{0.03}Mg_{0.03}Fe_{0.01}Ca_{0.01})_{\Sigma 2.04}(AsO_3OH)_{1.94}(SO_4)_{0.03}(PO_3OH)_{0.02} \cdot 5H_2O$. The crystal structure of honzaite was refined from powder X-ray data using Rietveld refinement ($R_p = 0.0116$, $R_{wp} = 0.0174$) of the structure model of isostructural burgessite. The structure of honzaite is based upon infinite chains of Ni octahedra and protonated As tetrahedra linked by a network of hydrogen bonds. Honzaite is the Ni-dominant analogue of burgessite. It is named in honor of the prominent Czech mineralogist and famous collector of minerals from the Jáchymov ore district, Dr. Jan "*Honza*" Hloušek (1950–2014). It forms during weathering of primary nickelskutterudite and tennantite under strongly acidic conditions.

Key-words: honzaite; new mineral; acid-arsenate; nickel; burgessite; oxide zone; Jáchymov; Czech Republic.

1. Introduction

During our systematic research focused chiefly on supergene minerals of the Jáchymov ore district in the Czech Republic, some rare and unusual minerals have been discovered (Hloušek *et al.*, 2014). One of the minerals is a new species, the Ni analogue of burgessite; in this paper, we report its description.

The mineral burgessite, $Co_2(AsO_3OH)_2(H_2O)_5$, was described for the first time from the Keeley Mine, South Lorrain Township, Ontario, Canada (Sejkora *et al.*, 2009) and it was also studied by Cooper & Hawthorne (2009) and Čejka *et al.* (2011). The second occurrence of this extremely rare mineral was described from the Jáchymov ore district by Sejkora & Macek (2014).

Honzaite is named in honor of the prominent Czech mineralogist and famous collector of minerals from the Jáchymov ore district, Dr. Jan "*Honza*" Hloušek (1950–2014). Thanks to his devoted collecting and scientific efforts, Jáchymov has become one of the richest localities, based on the number of discovered and well-described mineral species (more than 420) and it is justly considered a classic example of a Variscan hydrothermal ore deposit of the so-called five-element formation. Jan Hloušek discovered and co-authored descriptions of many new minerals from Jáchymov, including adolfpateraite, agricolaite, babánekite, běhounekite, geschieberite, ježekite, línekite, mathesiusite, metarauchite, ondrušite, plavnoite, slavkovite, svornostite, štěpite, švenekite and vysokýite. The name hloušekite was used for the Ni–Cu-dominant

0935-1221/18/0030-2770 $ 4.05
https://doi.org/10.1127/ejm/2018/0030-2770

member of the lindackerite supergroup (IMA 2013-048; Plášil *et al.*, 2014a). The pronunciation of *honzaite* using the International Phonic Alphabet is /hɒn zɑː aɪt'/.

The new mineral and name have been approved by the Commission on New Minerals, Nomenclature and Classification of the International Mineralogical Association (IMA2014-105). The holotype specimen (one 6 × 7 × 9 cm sample) is deposited in the collections of the Department of Mineralogy and Petrology of the National Museum in Prague, Cirkusová 1740, Praha 9, Czech Republic, catalog number P1N 38.099.

2. Occurrence

Honzaite was identified on one historical (probably 19th century) museum sample from the Jáchymov ore district (formerly St. Joachimsthal), Krušné hory Mountains, approximately 20 km north of Karlovy Vary, northwestern Bohemia, Czech Republic. The Jáchymov ore district is a classic example of Ag + As + Co + Ni + Bi and U vein-type hydrothermal mineralization. The ore veins cut a complex of medium-grade metasedimentary rocks of Cambrian to Ordovician age, in the envelope of a Variscan granite pluton. The majority of the ore minerals were deposited during Variscan mineralization from mesothermal fluids (Ondruš *et al.*, 2003a, b, d). Primary and supergene mineralization in this district resulted in extraordinarily varied associations; more than 420 minerals have been described from there, including an extremely diverse assemblage of supergene minerals (Ondruš *et al.*, 1997a, b and Ondruš *et al.*, 2003c, d; Hloušek *et al.*, 2014). During recent years, research on minerals from Jáchymov has been focused mainly on supergene minerals formed in abandoned mine adits (*e.g.*, Plášil *et al.*, 2012, Plášil *et al.*, 2013a, b, Plášil *et al.*, 2014b, Plášil *et al.*, 2015a, b, Plášil *et al.*, 2017; Kampf *et al.*, 2017) or in the oxide zone *in situ* (*e.g.* Sejkora *et al.*, 2011a, b, 2012; Plášil *et al.*, 2014a).

The new mineral honzaite was found in association with arsenolite, zeunerite, Ni-rich burgessite and a red amorphous phase with the approximate composition $(Co,Ni,Cu)_2(AsO_3OH)_2{\cdot}2H_2O$ (Sejkora & Macek, 2014). Honzaite formed during weathering of primary nickelskutterudite and tennantite disseminated in gangue, under strongly acidic conditions.

3. Physical properties and optical data

Honzaite occurs as irregular to hemispherical microcrystalline aggregates up to 5 mm in diameter (Fig. 1) on strongly weathered ore gangue. Tiny prismatic crystals (Fig. 2), up to 30 μm long, are rarely observed on the surfaces of these aggregates (Fig. 3). Honzaite has pale pink color, sometimes with purplish or violet tints. Its aggregates are opaque to translucent; individual crystals or tiny fragments are translucent to transparent. It has a pale pink streak and a vitreous luster. It does not fluoresce under either short- or long-wave ultraviolet light. Cleavage on {010} is good, the Mohs hardness is ~3, and the mineral is brittle with an irregular fracture. The density $D_{calc} = 2.993$ g/cm^3 was calculated on the basis of the empirical formula and unit-cell volume refined from powder data.

Fig. 1. Photomicrograph of microcrystalline aggregates of honzaite. Field of view 4.5 mm; photo J. Sejkora.

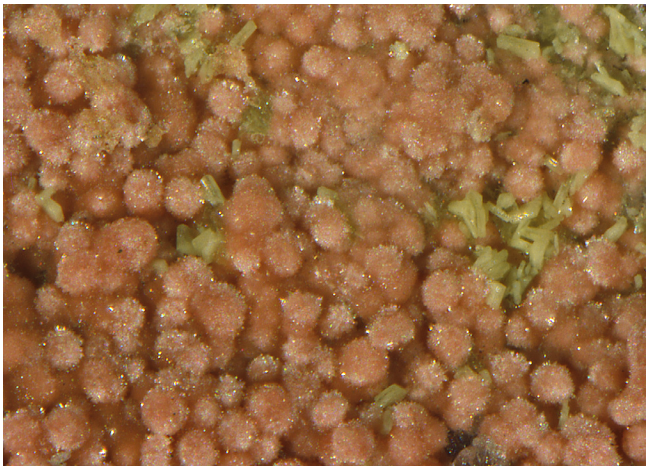

Fig. 2. Photomicrograph of the surface of aggregates of honzaite consisting of tiny prismatic crystals; the association includes greenish tabular crystals of Ni-containing zeunerite. Field of view 1 mm; photo J. Sejkora.

Honzaite is optically biaxial positive, with $\alpha = 1.601(2)$, $\beta = 1.608(2)$ and $\gamma = 1.629(2)$ (measured in white light), $2V_{meas.} = 60(1)°$ based on extinction data using EXCALIBR (Gunter *et al.*, 2004), $2V_{calc.} = 60.6°$. Dispersion could not be observed and honzaite exhibits no noticeable pleochroism. The Gladstone-Dale compatibility index $1-(K_P/K_C)$ is 0.008 for the empirical formula and unit-cell parameters from Rietveld refinement, indicating superior compatibility (Mandarino, 1981). The partially determined optical orientation is $X = \mathbf{b}$. Because the crystals are not of good enough quality for single-crystal X-ray diffraction study, the complete optical orientation could not be determined unambiguously. Assuming that the crystals are elongated on [100], $Z \wedge \mathbf{a} \approx 20°$, but it is

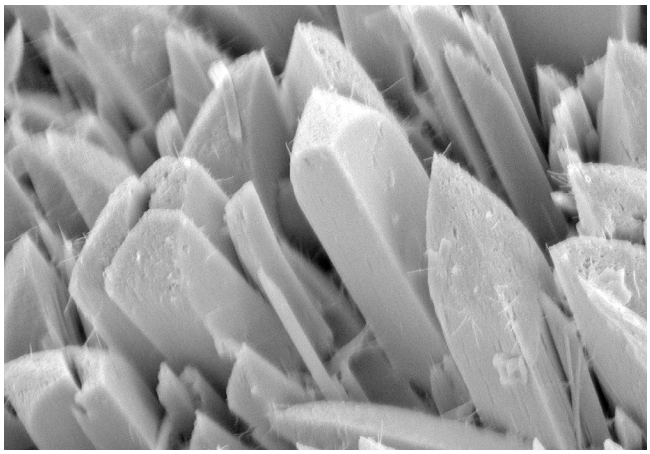

Fig. 3. Prismatic crystals of honzaite on the surface of its aggregates. Field of view 30 μm; scanning electron microscope picture J. Sejkora.

Table 1. Chemical composition of honzaite from Jáchymov (wt%).

Constituent	Mean 23 analyses	Range	SD
MgO	0.24	0.04–0.54	0.17
CaO	0.10	0.00–0.33	0.10
FeO	0.21	0.00–0.67	0.24
NiO	16.51	14.77–18.08	0.80
CoO	12.71	11.05–14.16	0.99
CuO	0.55	0.13–1.16	0.27
ZnO	0.84	0.20–1.65	0.36
P_2O_5	0.26	0.00–0.61	0.17
As_2O_5	45.82	43.60–48.62	1.23
SO_3	0.52	0.08–1.26	0.39
H_2O^*	22.15		
Total	99.91		

Note: content of H_2O^* was calculated on the basis of ideal composition derived from results of our crystal-structure study and by analogy with isostructural burgessite (Sejkora *et al.*, 2009; Cooper & Hawthorne, 2009).

uncertain whether this is in the obtuse or acute angle β. If it is in the acute angle β, it would be consistent with the orientation reported for burgessite: $X = \mathbf{b}$; $Y \wedge \mathbf{c} = 29°$ in β obtuse.

4. Chemical composition

Samples of honzaite were analyzed with a Cameca SX-100 electron microprobe (Laboratory of electron microscopy and microanalysis of the Masaryk University and Czech Geological Survey, Brno) operating in the wavelength-dispersion mode with an accelerating voltage of 15 kV, a specimen current of 4 nA, and a beam diameter of 15 μm. The following lines and standards were used: for *K*α, almandine (Fe), sanidine (Al, Si, K), metallic Co (Co), fluorapatite (P, Ca), Ni_2SiO_4 (Ni), gahnite (Zn), Mg_2SiO_4 (Mg), $SrSO_4$ (S), rhodonite (Mn), vanadinite (Cl, V); for *L*α, lammerite (Cu, As); for *L*β, metallic Sb (Sb), and for *M*α Pb (vanadinite). Counting times on peaks were 20 s for main elements and 60 s for minor elements, half of these values for each background. The raw intensities were converted to concentrations using the *PAP* (Pouchou & Pichoir, 1985) matrix-correction software. The elements Al, K, Mn, Pb, Sb, Si, V and Cl were sought, but found to be below the detection limit (about 0.01–0.03 wt%). Water content could not be analyzed directly because of the minute amount of material available. The presence and quantity of (OH) and (H_2O) groups were established by results of our crystal structure study and by analogy with isostructural burgessite (Cooper & Hawthorne, 2009).

Table 1 gives the chemical composition of honzaite from Jáchymov (mean of twenty-three determinations). Results of the chemical analyses correspond very well with the ideal formula $(Ni,Co)_2(AsO_3OH)_2{\cdot}5H_2O$, in which the *Ni+Co* site is dominantly occupied by Ni atoms (0.95–1.20 *apfu*). The contents of Co were found to be in the range 0.71–0.92 *apfu*; minor contents of other elements (Zn, Mg, Cu, Fe, Ca) do not exceed 0.03–0.10 *apfu*. In the tetrahedral site, only minor sulfur (up to 0.08 *apfu*) and phosphorus (up to 0.04 *apfu*) substitutes for As. The empirical formula of honzaite based on 13 O atoms per formula unit is $(Ni_{1.08}Co_{0.83}Zn_{0.05}Cu_{0.03}Mg_{0.03}Fe_{0.01}Ca_{0.01})_{\Sigma 2.04}(AsO_3OH)_{1.94}(SO_4)_{0.03}(PO_3OH)_{0.02}{\cdot}5H_2O$. The simplified formula is $(Ni,Co)_2(AsO_3OH)_2{\cdot}5H_2O$ and the ideal formula for the Co-free end-member is $Ni_2(AsO_3OH)_2{\cdot}5H_2O$, which requires NiO 30.66, As_2O_5 47.16, H_2O 22.18, total 100.00 wt%.

5. Raman and infrared spectroscopy

Honzaite was investigated with a confocal Raman microscope Nicolet DXR. The Raman signal was excited by a 532 nm laser and detected with a multichannel air-cooled CCD camera. The laser power at the sample was limited to 1 mW to avoid possible thermal destruction of the sample. Spectra were recorded between 2000 and 46 cm^{-1} with a spectral resolution of ±4 cm^{-1} and a minimum lateral resolution of ~1 μm on the sample (Fig. 4). The instrument was calibrated using a software-controlled calibration procedure employing multiple neon emission lines (wavelength calibration), multiple polystyrene Raman bands (laser frequency calibration) and standardized white-light sources (intensity calibration). Spectral manipulations were performed using the Omnic 9 software (Thermo Scientific). The main bands observed are (in wavenumbers): 1598, 853, 813, 742, 452, 386, 364, 326, 222, 174, 129 and 61 cm^{-1}. The tentative interpretation of vibrations of hydrogen-arsenate group $(AsO_3OH)^{2-}$ in the crystal structure of honzaite is based on papers by Keller (1971), Čejka *et al.* (2011), Frost *et al.* (2010b) and Sejkora *et al.* (2010). The band at 1598 cm^{-1} is connected with ν_2 (δ) bending vibrations of H_2O groups. The bands at 853 and 813 cm^{-1} can be assigned to the As–O stretching modes ν_1 and ν_3. The band at 742 cm^{-1} may be attributed to the ν As–OH stretching vibration. The band at 452 cm^{-1} is assigned to the triply degenerate ν_4 (As–O) and the bands 386, 364 and 326 cm^{-1} to the split double degenerate ν_2 (As–O) bending vibrations. The

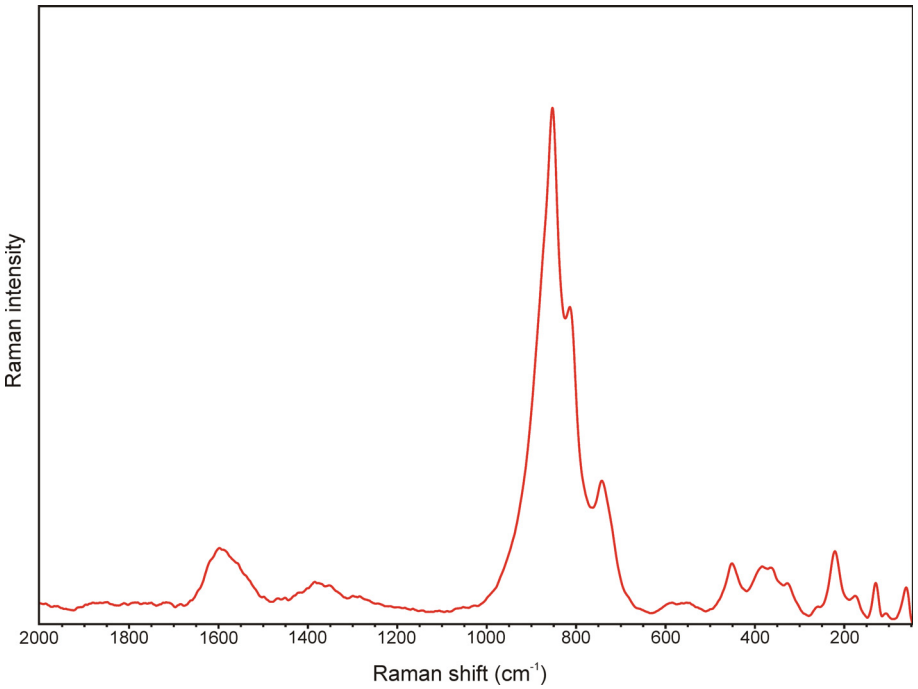

Fig. 4. Raman spectrum of honzaite.

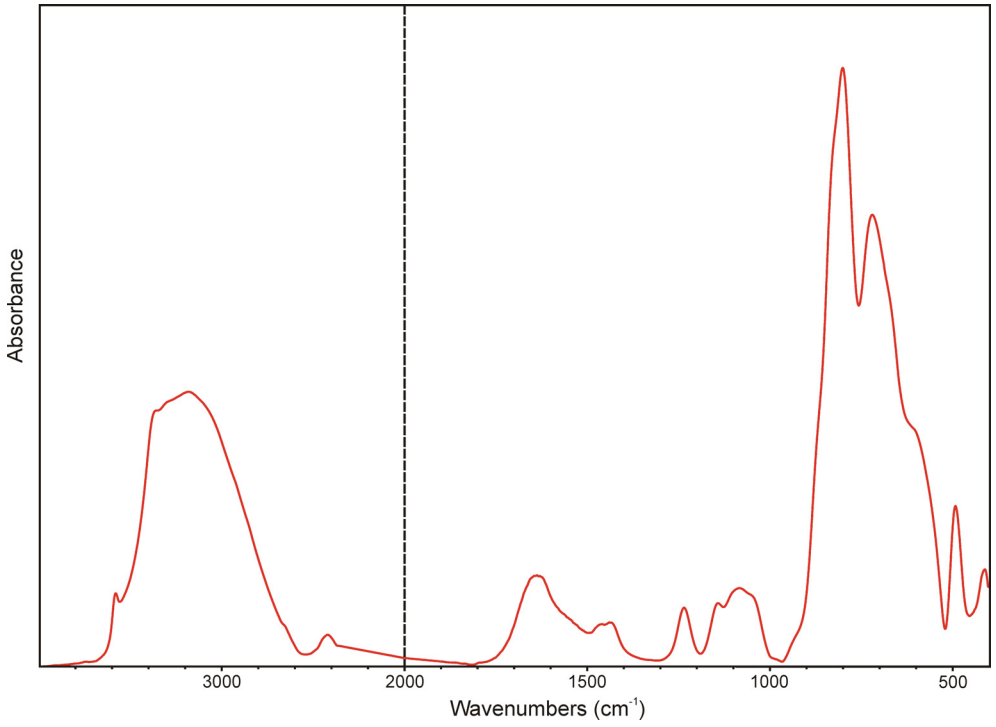

Fig. 5. Infrared spectrum of honzaite (splitted at 2000 cm^{-1}).

band at 222 cm^{-1} are assigned to the ν (O–H…O) stretching vibrations and bands in the region 180–50 cm^{-1} to lattice modes.

The infrared vibrational spectrum of honzaite was recorded by the ATR method on a Nicolet iS50 spectrometer (range 4000–400 cm^{-1}, resolution 4 cm^{-1}, 64 scans). The main bands (Fig. 5) observed are (in wavenumbers): 3582, 3366, 3177, 1640, 1233, 1147, 1082, 828, 801, 720, 604, 495 and 412 cm^{-1}. The infrared spectrum confirms the presence of water and hydroxyl ions in the structure (3366, 3177 and 1640 cm^{-1}), as well as the (AsO_3OH) groups: ν_3 asymmetric stretching mode and ν_1

symmetric stretching (828 and 801 cm^{-1}), ν_4 bending mode (495 cm^{-1}). The band at 3582 cm^{-1} may be connected with ν OH stretching vibration of the weakly bonded hydroxyl ion of the (AsO_3OH) units; a complex set of bands in the range from 1500 to 1050 cm^{-1} is assigned to the δ As–OH vibrations and overtones and combination bands. The band at 720 cm^{-1} are attributed to the As–OH stretching vibrations and band at 604 cm^{-1} is connected to libration modes or As-OH bending vibrations.

6. X-ray powder diffraction

Powder X-ray diffraction data for honzaite were collected on a Bruker D8 Advance diffractometer (National Museum, Prague) with a solid-state 1D LynxEye detector using Cu*K*α radiation and operating at 40 kV and 40 mA. The powder pattern was collected using Bragg–Brentano geometry in the range 3–60° 2θ, in 0.01° steps with a counting time of 30 s per step. Positions and intensities of reflections were found and refined using the PearsonVII profile-shape function with the ZDS program package (Ondruš, 1993) and the unit-cell parameters were refined by the least-squares algorithm implemented by Burnham (1962). The experimental powder pattern was indexed in line with the calculated values of intensities obtained from the crystal-structure refinement, based on Lazy Pulverix program (Yvon *et al.*, 1977). The experimental powder data given in Table 2 agree well with the pattern calculated from the single-crystal data for burgessite; experimental intensities are partly affected by preferred orientation (0*kk*) due to the long prismatic to acicular nature of the crystals. The refined unit-cell parameters of honzaite are: $a = 4.670(1)$, $b = 9.282(2)$, $c = 12.594(3)$ Å, $\beta = 99.14(1)°$ and $V = 539.0(1)$ Å^3.

7. Crystal-structure refinement

Because the honzaite crystals are not of good enough quality for single-crystal X-ray diffraction study, its structure was refined from powder data using the Rietveld method with the structure model of burgessite (Cooper & Hawthorne, 2009) as the starting point. Powder data were collected using a PANalytical Empyrean powder diffractometer equipped with a Cu X-ray tube and PIXcel^{3D} solid-state detector. Data collection employed Debye-Scherrer geometry in the 3–90° 2θ range with a step size 0.028° 2θ and a total counting time of 48 h using a scan accumulation option (40 scans). Before the measurement, the diffractometer was calibrated against a LaB_6 standard with the same settings. Rietveld refinement was carried out with Jana2006 software (Petříček *et al.*, 2014). Variables were background, shift, *FWHM* function, unit-cell parameters, atom coordinates and displacement parameters of Co/Ni, As and O atoms. Hydrogen atoms provided in the CIF for the structure of burgessite were not used in the Rietveld refinement. All refined and calculated values were corrected for correlations after Bérar & Lelann (1991). The final Rietveld plot is displayed in Fig. 6.

Table 2. X-ray powder diffraction data (*d* in Å) for honzaite.

I	$d_{meas.}$	$d_{calc.}$	*h*	*k*	*l*
100	7.431	7.438	0	1	1
18	6.215	6.217	0	0	2
2	5.164	5.165	0	1	$\bar{2}$
1	4.565	4.566	1	0	$\bar{1}$
1	4.338	4.348	0	2	1
2	4.137	4.129	1	1	0
2	4.102	4.115	1	0	$\bar{1}$
2	4.102	4.097	1	1	$\bar{1}$
1	3.783	3.784	0	1	3
1	3.754	3.762	1	1	1
9	3.717	3.719	0	2	$\bar{2}$
3	3.360	3.359	1	0	$\bar{3}$
7	3.254	3.255	1	2	$\bar{1}$
2	3.234	3.234	1	1	$\bar{2}$
3	3.159	3.158	1	1	$\bar{3}$
7	3.078	3.079	1	2	1
3	3.039	3.039	1	2	$\bar{2}$
5	3.005	3.002	0	3	1
2	2.948	2.948	0	1	4
1	2.864	2.864	1	0	3
1	2.769	2.770	0	3	2
3	2.737	2.737	1	1	$\bar{3}$
2	2.721	2.721	1	2	$\bar{3}$
2	2.674	2.673	1	1	$\bar{4}$
3	2.583	2.583	0	2	4
7	2.568	2.569	1	3	0
3	2.4787	2.4794	0	3	3
2	2.4730	2.4730	1	3	1
2	2.3520	2.3502	1	0	$\bar{5}$
1	2.3050	2.3054	2	0	0
1	2.2832	2.2830	2	0	$\bar{2}$
1	2.2173	2.2169	2	1	$\bar{2}$
1	2.1363	2.1363	1	2	4
1	2.1016	2.1020	1	3	3
1	2.0713	2.0728	1	4	0
3	2.0233	2.0248	0	4	3
3	2.0233	2.0213	1	4	1
3	2.0233	2.0225	0	1	$\bar{6}$
1	1.9670	1.9652	2	1	$\bar{4}$
1	1.9670	1.9677	1	1	$\bar{6}$
1	1.9384	1.9383	0	3	5
1	1.8799	1.8810	2	2	$\bar{2}$
1	1.8473	1.8451	2	2	$\bar{4}$
2	1.8362	1.8361	0	5	$\bar{1}$
2	1.8362	1.8370	2	3	$\bar{2}$
1	1.8051	1.8076	2	1	$\bar{5}$
1	1.7786	1.7788	0	5	$\bar{2}$
1	1.7228	1.7231	1	1	$\bar{7}$
1	1.7228	1.7221	1	5	0
1	1.7138	1.7127	1	3	5
1	1.6970	1.6962	2	1	$\bar{4}$
1	1.6861	1.6855	1	5	$\bar{2}$
1	1.6589	1.6589	0	2	$\bar{7}$
1	1.6518	1.6526	2	1	$\bar{6}$
1	1.6181	1.6171	2	2	4
1	1.6136	1.6136	2	3	$\bar{3}$
1	1.5835	1.5833	2	3	$\bar{5}$
1	1.5835	1.5835	2	4	$\bar{3}$

Refined unit-cell data for the monoclinic space group $P2_1/n$ are $a = 4.6736(6)$, $b = 9.296(1)$, $c = 12.592(1)$ Å, $\beta = 99.115(8)^0$ and $V = 540.2(1)$ Å^3. The final indices of

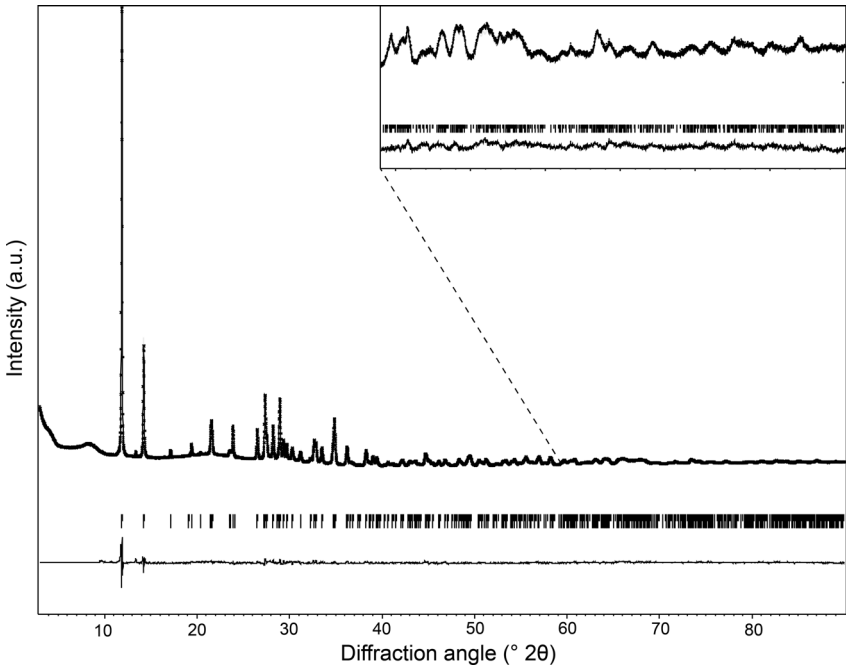

Fig. 6. Final Rietveld plot showing observed (asterisks), calculated (full line) and difference profiles of the refinement of the crystal structure from powder X-ray data.

Table 3. Summary of data-collection conditions and Rietveld refinement parameters for honzaite.

Crystal data	
System	Monoclinic
Space group	$P2_1/n$
Unit-cell parameters	
	$a = 4.6736(6)$ Å
	$b = 9.2960(11)$ Å
	$c = 12.5923(11)$ Å
	$\beta = 99.115(8)°$
	$V = 540.17(11)$ Å^3
Z	2
Density (calculated)	2.923 g · cm^{-3}
Sample	Powder, 0.3 mm Ø capillary
Absorption correction, μ (Cu$K\alpha$)	Cylindrical sample, 20.75 mm^{-1}
Source, wavelength	PANalytical Empyrean, Cu$K\alpha_{1,2}$
θ range for data collection [°], step size [°]	3–90, 0.028
Refinement software	Jana2006 (Petříček *et al.*, 2014)
Refinement method	Rietveld refinement
Profile function	Pseudo-Voigt
Data/obs/restraints/parameters	6192/437/0/54
R_p, R_{wp}	0.0116, 0.0173
R_F, R_{Bragg}	0.0557, 0.0843
GOF, χ^2	3.07, 9.43
$\Delta\ \rho_{max}/\Delta\ \rho_{min}$	0.64 and −0.52 e·Å^{-3}

agreement provided quite satisfactory values: $R_p = 0.0116$, $R_{wp} = 0.0174$, $R_{exp} = 0.0056$, $R_F = 0.0557$ (see Tables 3, 4 and 5)

The Rietveld refinement from the experimental powder data provided very similar results to those given by Cooper & Hawthorne (2009) for the structure of burgessite. Honzaite and burgessite are expected to be isostructural, based on the similar stereochemistry of Co and Ni, and our study confirms that. As for burgessite, the structure of honzaite (Fig. 7) contains a single site occupied by Ni (dominantly, according to EMPA) and lesser amounts of Co and Zn (for the model intensities, only Co was considered and the occupancy was not refined due to similar scattering power for X-rays), one As and seven O sites in the asymmetric unit. According to bond valence analysis (Table 4), three of the O sites correspond to molecular H_2O, and one is an OH^- group of the protonated $AsO_3(OH)$ tetrahedron.

8. Further discussion

Honzaite is isostructural with the mineral burgessite, $Ni_2(AsO_3OH)_2{\cdot}5H_2O$ (Sejkora *et al.*, 2009; Cooper & Hawthorne, 2009). The most important difference is in the crystal chemistry, the dominant element in the octahedral cation site is Ni (honzaite) or Co (burgessite). Comparative data for the two minerals are given in Table 6. The occurrence of Ni-rich burgessite (Sejkora & Macek, 2014) indicates probable solid solution between honzaite and burgessite (Fig. 8). We note that the pink color of honzaite is probably due to substantial, but subordinate, Co content; the pure Ni end-member would be green.

The origin of honzaite, is the case for the coexisting Ni-rich burgessite, is related to the weathering of primary nickelskutterudite and tennantite. The presence of the hydrogen-arsenate group in the crystal structure of honzaite indicates strongly acidic conditions for its formation; as is the case for other hydrogen-arsenate minerals known from this ore district, *e.g.* geminite (Sejkora *et al.*, 2010), koritnigite (Frost *et al.*, 2011),

Table 4. Atom positions, occupancies, equivalent displacement parameters (U_{eq}; in Å^2), anisotropic displacement parameters and bond-valence sums (in valence units, *vu*) for honzaite.

	x	*y*	*z*	*U*(eq)*	U^{11}	U^{22}	U^{33}	U^{12}	U^{13}	U^{23}	*BV*
Ni/Co#	0.451(3)	0.4598(18)	0.3780(13)	0.064(11)	0.065(18)	0.068(17)	0.06(2)	0.001(14)	0.012(13)	−0.006(15)	2.14(12)
As	0.485(3)	0.1880(13)	0.0322(11)	0.057(7)	0.047(10)	0.053(11)	0.077(12)	−0.003(12)	0.024(8)	−0.015(13)	5.3(4)
O1	0.148(11)	0.626(6)	0.363(4)	0.04(3)*							1.7(2)
O2	0.282(13)	0.411(6)	0.519(5)	0.05(2)*							1.9(2)
O3	0.752(10)	0.301(7)	0.417(4)	0.059(19)*							1.66(17)
O4	0.589(10)	0.352(6)	0.074(4)	0.04(2)*							1.35(19)
O5	0.621(8)	0.525(5)	0.248(4)	0.021(19)*							0.39(4)
O6	0.181(9)	0.327(6)	0.279(3)	0.04(2)*							0.37(3)
O7	0.44(2)	0.048(13)	0.428(7)	0.11(7)*							0

Ni/Co occupancies set to 0.55 and 0.45, respectively.
* *U*(eq) is defined as a third of the trace of the orthogonalized U_{ij} tensor.

Table 5. Selected bond distances (in Å) in the crystal structure of honzaite.

As–O1^{ii}	1.65(6)	Ni/Co–O1	2.09(5)
As–O2^{iii}	1.69(6)	Ni/Co–O2	2.10(7)
As–O3^{iv}	1.67(5)	Ni/Co–O2^{i}	2.04(6)
As–O4	1.66(5)	Ni/Co–O3	2.04(6)
⟨As–O⟩	1.67	Ni/Co–O5	2.02(5)
		Ni/Co–O6	2.04(5)
		⟨*Me*–O⟩	2.06
O1–O2	2.81(8)	O2–O4^{viii}	2.73(8)
O1–O2^{v}	2.71(9)	O2–O5^{i}	2.97(8)
O1–O2^{i}	2.86(7)	O3–O4^{ix}	2.72(7)
O1–O3^{i}	2.82(7)	O3–O5	2.97(7)
O1–O4^{vi}	2.56(8)	O3–O6	2.95(6)
O1–O5^{vii}	2.82(6)	O3–O6^{x}	2.86(7)
O1–O5	2.98(7)	O3–O7	2.80(13)
O1–O6	2.99(7)	O4–O5	2.70(7)
O1–O6^{vi}	2.79(7)	O4–O7^{xi}	2.88(12)
O2–O2^{i}	2.72(8)	O4–O7^{iii}	2.79(12)
O2–O3^{vii}	2.79(8)	O5–O6	2.84(7)
O2–O3	2.90(8)	O7–O7^{xii}	2.01(13)
O2–O3i	2.81(8)		

Symmetry codes: (i) $-x+1, -y+1, -z+1$; (ii) $-x+1/2, y-1/2, -z+1/2$; (iii) $x+1/2, -y+1/2, z-1/2$; (iv) $x-1/2, -y+1/2, z-1/2$; (v) $-x, -y+1, -z+1$; (vi) $-x+1/2, y+1/2, -z+1/2$; (vii) $x-1, y, z$; (viii) $x-1/2, -y+1/2, z+1/2$; (ix) $x+1/2, -y+1/2, z+1/2$; (x) $x+1, y, z$; (xi) $-x+3/2, y+1/2, -z+1/2$; (xii) $-x+1, -y, -z+1$.

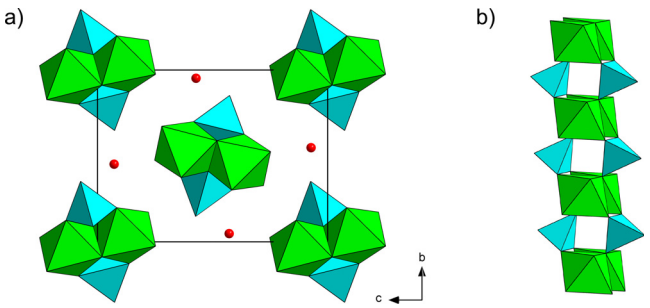

Fig. 7. View of the structure of honzaite: (a) along **a**, (Ni, Co)$(H_2O)_2O_4$ octahedra displayed in green, AsO_3OH groups are azure blue. The H_2O molecules that are not linked to metal cation sites are displayed in red; (b) the infinite chain formed by octahedrally coordinated Ni/Co atoms (dominant Ni in honzaite, Co in burgessite) and protonated $AsO_3(OH)$ groups (azure blue).

haidingerite and brassite (Frost *et al.*, 2010a) or pharmacolite (Frost *et al.*, 2010b). At Jáchymov, the predominant supergene minerals of nickel (Ondruš *et al.*, 1997a) are annabergite and other Ni-containg members of the vivianite group or locally also Ni-sulfates (nickel-hexahydrite, retgersite, morenosite).

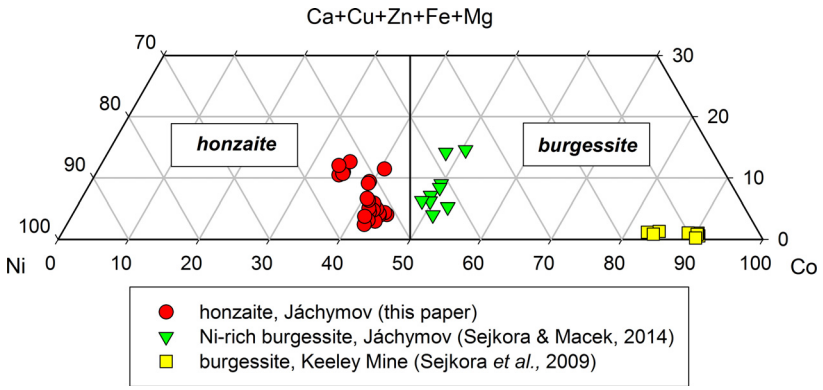

Fig. 8. Compositional variations (atomic proportions) in minerals of the honzaite–burgessite solid solution.

Table 6. Comparative data for honzaite and burgessite (Sejkora *et al.*, 2009; Cooper & Hawthorne, 2009).

	Honzaite	Burgessite
Formula (ideal)	$Ni_2(AsO_3OH)_2 \cdot 5H_2O$	$Co_2(AsO_3OH)_2 \cdot 5H_2O$
Symmetry	monoclinic, $P2_1/n$	monoclinic, $P2_1/n$
Unit-cell	$a = 4.670(1)$, $b = 9.282(2)$, $c = 12.594(3)$ Å, $\beta = 99.14(1)°$ $V = 539.0(1)$ Å^3	$a = 4.706(1)$, $b = 9.299(3)$, $c = 12.738(4)$ Å, $\beta = 98.933(8)°$ $V = 550.6(5)$ Å^3
Z	2	2
Strongest powder pattern lines d, I, hkl	7.431, 100 (0 1 1) 6.215, 18 (0 0 2) 3.717, 9 (6 0 0) 3.254, 7 (12 $\bar{1}$) 3.078, 7 (1 2 1) 2.568, 7 (1 3 0)	7.446, 100 (0 1 1) 6.267, 44 (0 0 2) 3.725, 29 (0 2 2) 3.260, 25 (12 $\bar{1}$) 2.998, 31 (0 3 1) 2.970, 21 (0 1 4) 2.596, 23 (0 2 4)
Optics	biaxial (+) $\alpha = 1.601$, $\beta = 1.608$, $\gamma = 1.629$	biaxial (+) $\alpha = 1.596$, $\beta = 1.604$, $\gamma = 1.628$

Acknowledgements: The authors wish to express their thanks to Radek Škoda (Masaryk University, Brno) and Ján Pásztor (Nicolet CZ s.r.o., Prague) for their kind support in this study. Igor Pekov and an anonymous reviewer, as well as editor-in-chief Sergey Krivovichev, are acknowledged for valuable comments and suggestions that helped to improve the manuscript. This work was financially supported by Czech Science Foundation (project GACR 17-09161S).

References

Bérar, J.-F. & Lelann, P. (1991): E.s.d.'s and estimated probable errors obtained in Rietveld refinements with local correlations. *J. Appl.Cryst.*, **24**, 1–5.

Burnham, C.W. (1962): Lattice constant refinement. Carnegie Institute Washington Yearbook, **6**, 132–135.

Cooper, M.A. & Hawthorne, F.C. (2009): The crystal structure of burgessite, $Co_2(H_2O)_4[AsO_3(OH)]_2(H_2O)$, and its relation to erythrite. *Can. Mineral.*, **17**, 165–172.

Čejka, J., Sejkora, J., Bahfenne, S., Palmer, S.J., Plášil, J., Frost, R. L. (2011): Raman spectroscopy of hydrogene-arsenate group (AsO_3OH) in solid-state compounds: cobalt mineral phase burgessite $Co_2(H_2O)_4[AsO_3OH]_2 \cdot H_2O$. *J. Raman Spectrosc.*, **42**, 214–218.

Frost, R.L., Bahfenne, S., Čejka, J., Sejkora, J., Palmer, S.J., Škoda, R. (2010a): Raman microscopy of haidingerite $Ca(AsO_3OH) \cdot H_2O$ and brassite $Mg(AsO_3OH) \cdot 4H_2O$. *J. Raman Spectrosc.*, **41**, 690–693.

Frost, R.L., Bahfenne, S., Čejka, J., Sejkora, J., Plášil, J., Palmer, S. J. (2010b): Raman spectroscopic study of the hydrogen-arsenate mineral pharmacolite $Ca(AsO_3OH) \cdot 2H_2O$ – implications for aquifer and sediment remediation. *J. Raman Spectrosc.*, **41**, 1348–1352.

Frost, R.L., Sejkora, J., Čejka, J., Plášil, J., Bahfenne, S., Keeffe, E. C. (2011): Raman spectroscopy of hydrogen arsenate group $(AsO_3OH)^{2-}$ in solid-state compounds: cobalt-containing zinc arsenate mineral, koritnigite $(Zn,Co)(AsO_3OH) \cdot H_2O$. *J. Raman Spectrosc.*, **42**, 534–539.

Gunter, M.E., Bandli, B.R., Bloss, F.D., Evans, S.H., Su, S.C., Weaver, R. (2004): Results from a McCrone spindle stage short course, a new version of EXCALIBR, and how to build a spindle stage. *Microscope*, **52**, 23–39.

Hloušek, J., Plášil, J., Sejkora, J., Škácha, P. (2014): News and new minerals from Jáchymov, Czech Republic (2003–2014). *Bull. mineral.-petrolog. Odd. Nár. Muz.* (Praha), **22**, 155–181. (in Czech).

Kampf, A.R., Sejkora, J., Witzke, T., Plášil, J., Čejka, J., Nash, B.P., Marty, J. (2017): Rietveldite, $Fe(UO_2)(SO_4)_2(H_2O)_5$, a new uranyl sulfate mineral from Giveaway-Simplot mine (Utah, USA), Willi Agatz mine (Saxony, Germany) and Jachymov (Czech Republic). *J. Geosci.*, **62**, 107–120.

Keller, P. (1971): Kristallchemie der Phosphat- und Arsenat-Minerale unter besonderer Berücksichtigung der Kationen-Koordinationspolyeder und des Kristallwassers. Teil. I: Die Anionen der Phosphat- und Arsenatminerale. *N. Jb. Mineral. Mh.*, **1971**, 491–510

Mandarino, J.A. (1981): The Gladstone-Dale relationship: Part IV. The compatibility concept and its application. *Can. Mineral.*, **19**, 441–450.

Ondruš, P. (1993): A computer program for analysis of X-ray powder diffraction patterns. Materials Science Forum, EPDIC-2, Enchede, **133–136**, pp. 297–300.

Ondruš, P., Veselovský, F., Hloušek, J., Skála, R., Frýda, J., Čejka, J., Gabašová, A. (1997a): Secondary minerals of the Jáchymov (Joachimsthal) ore district. *J. Czech Geol. Soc.*, **42**, 3–76.

Ondruš, P., Veselovský, F., Skála, R., Císařová, I., Hloušek, J., Frýda, J., Vavřín, I., Čejka, J., Gabašová, A. (1997b): New naturally occurring phases of secondary origin from Jáchymov (Joachimsthal). *J. Czech Geol. Soc.*, **42**, 77–107.

Ondruš, P., Veselovský, F., Gabašová, A., Drábek, M., Dobeš, P., Malý, K., Hloušek, J., Sejkora, J. (2003a): Ore-forming processes and mineral parageneses of the Jáchymov ore district. *J. Czech Geol. Soc.*, **48**, 157–192.

Ondruš, P., Veselovský, F., Gabašová, A., Hloušek, J., Šrein, V. (2003b): Geology and hydrothermal vein system of the Jáchymov (Joachimsthal) ore district. *J. Czech Geol. Soc.*, **48**, 3–18.

Ondruš, P., Veselovský, F., Gabašová, A., Hloušek, J., Šrein, V. (2003c): Supplement to secondary and rock-forming minerals of the Jáchymov ore district. *J. Czech Geol. Soc.*, **48**, 149–155.

Ondruš, P., Veselovský, F., Gabašová, A., Hloušek, J., Šrein, V., Vavřín, I., Skála, R., Sejkora, J., Drábek, M. (2003d): Primary minerals of the Jáchymov ore district. *J. Czech Geol. Soc.*, **48**, 19–147.

Petříček, V., Dušek, M., Palatinus, L. (2014): Crystallographic computing system JANA2006: general features. *Zeit. Krist.*, **229**, 345–352.

Plášil, J., Hloušek, J., Veselovský, F., Fejfarová, K., Dušek, M., Škoda, R., Novák, M., Čejka, J., Sejkora, J., Ondruš, P. (2012): Adolfpateraite, $K(UO_2)(SO_4)(OH)(H_2O)$, a new uranyl sulphate mineral from Jáchymov, Czech Republic. *Am. Mineral*., **97**, 447–454.

Plášil, J., Fejfarová, K., Hloušek, J., Škoda, R., Novák, M., Sejkora, J., Čejka, J., Dušek, M., Veselovský, F., Ondruš, P., Majzlan, J., Mrázek, Z. (2013a): Štěpite, $U(AsO_3OH)_2 \cdot 4H_2O$, from Jáchymov, Czech Republic: the first natural arsenate of tetravalent uranium. *Mineral. Mag.*, **77**, 137–152.

Plášil, J., Hloušek, J., Škoda, R., Novák, M., Sejkora, J., Čejka, J., Veselovský, F., Majzlan, J. (2013b): Vysokýite, $U^{4+}[AsO_2(OH)_2]_4 \cdot 4H_2O$, a new mineral from Jáchymov, Czech Republic. *Mineral. Mag.*, **77**, 3055–3066.

Plášil, J., Sejkora, J., Škoda, R., Novák, M., Kasatkin, A.V., Škácha, P., Veselovský, F., Fejfarová, K., Ondruš, P. (2014a): Hloušekite, $(Ni, Co)Cu_4(AsO_4)_2(AsO_3OH)_2(H_2O)_9$, a new member of the lindackerite supergroup from Jáchymov, Czech Republic. *Mineral. Mag.*, **78**, 1341–1353.

Plášil, J., Veselovský, F., Hloušek, J., Škoda, R., Novák, M., Sejkora, J., Čejka, J., Škácha, P., Kasatkin, A.V. (2014b): Mathesiusite, $K_5(UO_2)_4(SO_4)_4(VO_5)(H_2O)_4$, a new uranyl sulfate mineral from Jáchymov, Czech Republic. *Am. Mineral.*, **99**, 625–663.

Plášil, J., Hloušek, J., Kasatkin, A.V., Belakovskiy, D.I., Čejka, J., Chernyshov, D. (2015a): Ježekite, $Na_8[(UO_2)(CO_3)_3](SO_4)_2 \cdot 3H_2O$, a new uranyl mineral from Jáchymov, Czech Republic. *J. Geosci.*, **60**, 259–267.

Plášil, J., Hloušek, J., Kasatkin, A.V., Novák, M., Čejka, J., Lapčák, L. (2015b): Svornostite, $K_2Mg[(UO_2)(SO_4)_2]_2\ 8H_2O$, a new uranyl sulfate mineral from Jáchymov, Czech Republic. *J. Geosci.*, **60**, 113–121.

Plášil, J., Škácha, P., Sejkora, J., Kampf, A.R., Škoda, R., Čejka, J., Hloušek, J., Kasatkin, A.V., Pavlíček R., Babka, K. (2017): Plavnoite, a new K–Mn member of the zippeite group from Jáchymov, Czech Republic. *Eur. J. Mineral.*, **29**, 117–128.

Pouchou, J.L. & Pichoir, F. (1985) "PAP" (ϕρZ) procedure for improved quantitative microanalysis. *in* "Microbeam Analysis", J.T. Armstrong, ed. San Francisco Press, San Francisco, 104–106.

Sejkora, J. & Macek, I. (2014): Burgessite, a new mineral for the Jáchymov ore district (Czech Republic). *Bull. mineral.-petrolog. Odd. Nár. Muz.* (Praha), **22**, 221–226. (in Czech).

Sejkora, J., Čejka, J., Frost, R.L., Bahfenne, S., Plášil, J., Keeffe, E. C. (2010): Raman spectroscopy of hydrogen-arsenate group (AsO_3OH) in solid-state compounds: copper mineral phase geminite $Cu(AsO_3OH) \cdot H_2O$ from different geological environments. *J. Raman Spectrosc.*, **41**, 1038–1043.

Sejkora, J., Hawthorne, F.C., Cooper, M.A., Grice, J. D., Vajdak, J., Jambor, J.L. (2009): Burgessite, $Co_2(H_2O)_4[AsO_3(OH)]_2(H_2O)$, a new arsenate mineral species from the Keeley mine, South Lorrain township, Ontario, Canada. *Can. Mineral.*, **47**, 159–164.

Sejkora, J., Plášil, J., Císařová, I., Škoda, R., Hloušek, J., Veselovský, F., Jebavá, I.(2011a): Interesting supergene Pb-rich mineral association from the Rovnost mining field, Jáchymov (St. Joachimsthal), Czech Republic. *J. Geosci.*, **56**, 257–271.

Sejkora, J., Plášil, J., Veselovský, F., Císařová, I., Hloušek, J. (2011b): Ondrušite, $CaCu_4(AsO_4)_2(AsO_3OH)_2 \cdot 10H_2O$, a new mineral species from the Jáchymov ore district, Czech Republic: description and crystal-structure determination. *Can. Mineral.*, **49**, 885–897.

Sejkora, J., Babka, K., Pavlíček, R. (2012): Saléeite from the uranium ore district Jáchymov (Czech Republic). *Bull. mineral.-petrolog. Odd. Nár. Muz.* (Praha), **20**, 208–212. (in Czech).

Yvon, K., Jeitschko, W., Parthé, E. (1977): Lazy Pulverix, a computer program for calculation X-ray and neutron diffraction powder patterns. *J. Appl. Cryst.*, **10**, 73–74.

Received 25 August 2017
Modified version received 30 December 2017
Accepted 6 January 2018